Concentric Cone Antihydrogen Gravity Experiment

S.S. Patel[1, b)], S.R. Sun[1], and C.A. Ordonez[1, a)]

[1]*Department of Physics, University of North Texas, Denton, Texas 76203-5017, United States.*

[a)]Corresponding author: cao@unt.edu
[b)]sahil.patelsp@gmail.com

Abstract. An antihydrogen gravity experiment is proposed that could be conducted at the CERN Antiproton Decelerator facility to determine the directionality of the acceleration of antihydrogen in earth's gravitational field. The experiment would consist of an antihydrogen source located in a cylindrical vacuum chamber at the common vertex of an azimuthally symmetric series of concentric detector cones. Within any region bounded by two consecutive detector cones, the antihydrogen cannot undergo linear motion and annihilate with either detector cone. However, with parabolic trajectories, such as those of objects under the influence of gravity, the antihydrogen can annihilate with a detector cone, the position of which relative to the other detector cones being an indication of the direction of the gravitational acceleration of antihydrogen. An optimization of the configuration of the experiment is performed and the probability of antihydrogen annihilating with the detector cones determined. For purposes of simplicity, the model considers the antihydrogen to be a point source at a temperature of 4 K.

INTRODUCTION

No experimental evidence has ever been reported that definitively indicates the gravitational interaction between matter and antimatter. Various collaborations at CERN, including AEGIS,[1] ALPHA,[2] and GBAR,[3] are developing and conducting experiments to study the gravitational properties of antimatter. An antihydrogen gravity experiment is proposed that could potentially be used to determine the direction of the acceleration of antihydrogen due to earth's gravity. Prior research at the University of North Texas has considered aperture-based antihydrogen gravity experiments.[4,5] In the present study, the experimental configuration consists of an azimuthally symmetric series of concentric detector cones enclosed by a cylindrical ultra-high vacuum chamber, as shown in Fig. 1. It is assumed that a point antihydrogen source is located at the common vertex of the detector cones and further that the detector cones themselves are of infinitesimal width. For an antiatom to enter any region bounded by two adjacent detector cones, the direction of the antiatom's initial velocity must be strictly within the bounds of the region. As such, an antiatom cannot follow a straight-line trajectory and annihilate with a detector cone. Detection is only possible if the trajectory of an antiatom is influenced by gravity, provided that all other forces acting upon the antiatom are negligible. If annihilations occur on the lower surfaces of the detector cones, antihydrogen gravitationally accelerates away from the earth. If annihilations occur on the upper surfaces of the detector cones, antihydrogen gravitationally accelerates towards the earth. It is assumed here that a detector (along with an advanced computer algorithm) that can distinguish sufficiently between antihydrogen annihilations and cosmic rays would be used, similar to the silicon vertex detector used by the ALPHA collaboration.[6]

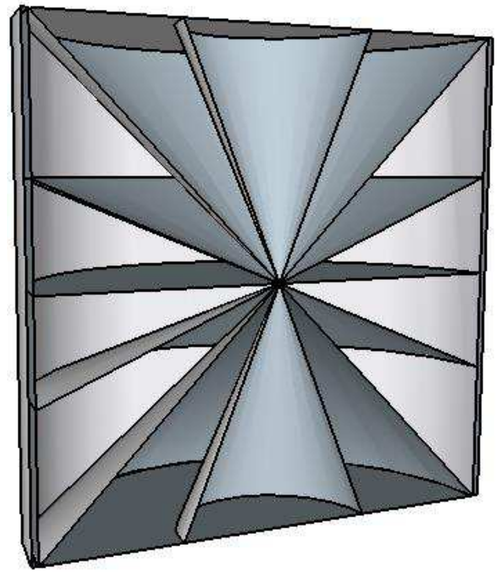

FIGURE 1. Cross-sectional view of the concentric cone antihydrogen gravity experiment.

MONTE CARLO SIMULATION

The Monte Carlo method is used to simulate the antihydrogen gravity experiment. A Cartesian coordinate system consisting of spatial coordinates (x, y, z) and corresponding unit vectors $(\hat{\boldsymbol{i}}, \hat{\boldsymbol{j}}, \hat{\boldsymbol{k}})$ is defined such that the z-axis coincides with the axis of symmetry of the apparatus, and the coordinate origin is located at the common vertex of the concentric detector cones, or equivalently the point antihydrogen source. The initial Cartesian position coordinates of each antiatom are then $x_0 = y_0 = z_0 = 0$. The antiatom's initial Cartesian velocity components, v_{0x}, v_{0y}, and v_{0z}, are sampled from a Maxwellian velocity distribution of mean zero and standard deviation given by the thermal speed, $v_t = \sqrt{kT/m}$, with k being the Boltzmann constant, T the temperature of the antihydrogen source, and m the mass of an antihydrogen atom. As a consequence of the system's azimuthal symmetry, all variables can be considered within the rz-plane of a cylindrical coordinate system, as shown in Fig. 2. The Cartesian coordinates x and y are converted into the cylindrical coordinate r by $x^2 + y^2 = r^2$. Hence, the radial coordinate of an antiatom's initial position is $r_0 = 0$ whereas the radial component of its initial velocity is $v_{0r} = \sqrt{v_{0x}^2 + v_{0y}^2}$. The null hypothesis that the gravitational acceleration of antimatter is identical in both magnitude and direction to that of matter is assumed, such that each antiatom experiences an acceleration due to gravity given by $\boldsymbol{g} = -g\hat{\boldsymbol{k}}$, with g denoting the magnitude of the gravitational acceleration for matter. The governing equations of motion in cylindrical coordinates are then

$$r(t) = r_0 + v_{0r}t = v_{0r}t \tag{1}$$

$$z(t) = z_0 + v_{0z}t - \frac{gt^2}{2}, \tag{2}$$

where $r(t)$ and $z(t)$ are the respective radial and axial displacements of an antiatom relative to the coordinate origin at time t. An equation for the antiatom's trajectory that expresses z as a function of r is derived by solving for t in Eq. (1) to give $t = r/v_{0r}$ and substituting the resulting expression into Eq. (2),

$$z = \frac{rv_{0z}}{v_{0r}} - \frac{gr^2}{2v_{0r}^2}. \tag{3}$$

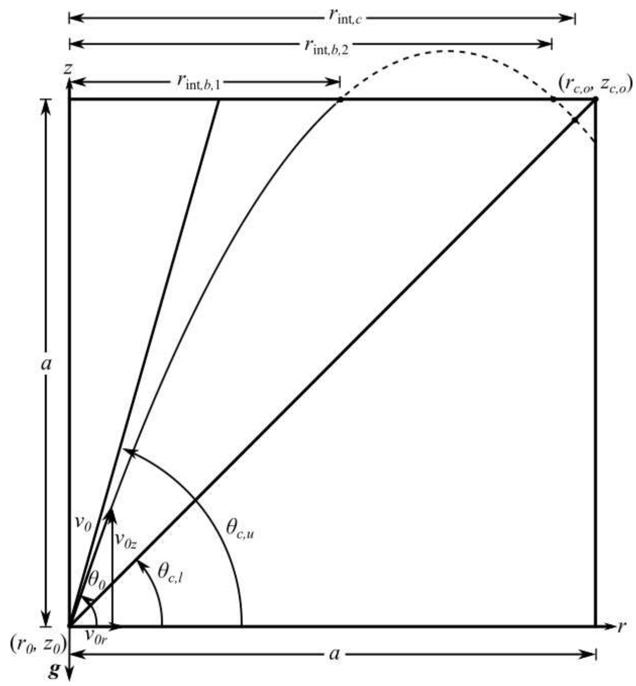

FIGURE 2. Diagram of the relevant variables of the Monte Carlo simulation in the rz -plane for $z \geq 0$.

The initial direction of motion for each antiatom is characterized by the angle $\theta_0 = \arctan(v_{0z} / v_{0r})$, measured with respect to the r -axis. To analyze antiatom motion and annihilation, the rz -plane is partitioned into mutually independent sectors defined by any two adjacent detector cones. Therefore, the minimum angle at which an antiatom can enter a certain sector, $\theta_{s,\min}$, is the angle of the lower detector cone, $\theta_{c,l}$, or $-\pi / 2$ if no lower detector cone exists for the sector, and the maximum such entry angle, $\theta_{s,\max}$, is the angle of the upper detector cone, $\theta_{c,u}$, or $\pi / 2$ if no upper detector cone exists for the sector:

$$\theta_{s,\min} = \begin{cases} \theta_{c,l}, & \theta_{c,l} \textit{ exists} \\ -\dfrac{\pi}{2}, & \theta_{c,l} \textit{ does not exist} \end{cases} \tag{4}$$

$$\theta_{s,\max} = \begin{cases} \theta_{c,u}, & \theta_{c,u} \textit{ exists} \\ \dfrac{\pi}{2}, & \theta_{c,u} \textit{ does not exist.} \end{cases} \tag{5}$$

A sector that satisfies $\theta_{s,\min} < \theta_0 < \theta_{s,\max}$ is thus the sector within which the motion and annihilation of an antiatom exclusively occurs.

Given that the gravitational acceleration of antimatter is presumed to be directed towards the center of the earth, detection is evaluated as the annihilation of an antiatom with the upper surface of the lower detector cone of its corresponding sector. In the rz -plane, the equation of the lower detector cone is

$$z = r \tan \theta_{c,l}, \tag{6}$$

whereas the equations of the lower, lateral, and upper chamber boundaries are

$$z = -a \tag{7}$$

$$r = a \tag{8}$$

$$z = a, \tag{9}$$

respectively, with a representing the dimension that defines both the radius and half-height of the vacuum chamber. The inner endpoint of a lower detector cone is located at the coordinate origin by definition, and the outer endpoint is found by solving for the point of intersection between the equation of the lower detector cone, Eq. (6), and that of appropriate chamber boundary depending on $\theta_{c,l}$, either Eq. (7) for $-\pi/2 < \theta_{c,l} < -\pi/4$, Eq. (8) for $|\theta_{c,l}| < \pi/4$, or Eq. (9) for $\pi/4 < \theta_{c,l} < \pi/2$, to give the endpoint coordinates

$$r_{c,o} = \begin{cases} a, & |\theta_{c,l}| \le \pi/4 \\ \dfrac{a}{\tan\theta_{c,l}}, & \theta_{c,l} > \pi/4 \\ -\dfrac{a}{\tan\theta_{c,l}}, & \theta_{c,l} < -\pi/4 \end{cases} \tag{10}$$

$$z_{c,o} = \begin{cases} a\tan\theta_{c,l}, & |\theta_{c,l}| \le \pi/4 \\ a, & \theta_{c,l} > \pi/4 \\ -a, & \theta_{c,l} < -\pi/4. \end{cases} \tag{11}$$

For detection to occur, an antiatom's trajectory and a lower detector cone must intersect within the vacuum chamber at a point other than the coordinate origin. To determine the radial coordinate of this point of intersection, $r_{\text{int},c}$, Eqs. (3) and (6) are evaluated at $r = r_{\text{int},c}$ and accordingly equated to each other,

$$\frac{r_{\text{int},c} v_{0z}}{v_{0r}} - \frac{g r_{\text{int},c}^2}{2 v_{0r}^2} = r_{\text{int},c} \tan\theta_{c,l}. \tag{12}$$

Solving for $r_{\text{int},c}$ yields two solutions, one of which is the coordinate origin. The other solution is the relevant solution:

$$r_{\text{int},c} = \frac{2 v_{0r} (v_{0z} - v_{0r} \tan\theta_{c,l})}{g}. \tag{13}$$

If $0 < r_{\text{int},c} \le r_{c,o}$, then $r = r_{\text{int},c}$ is a potential candidate for the site of annihilation. However, this conclusion alone is insufficient to confirm detection if the respective sector of an antiatom is such that $\theta_{s,\max} > \pi/4$, as it is possible in this case for the antiatom to annihilate with the upper chamber boundary prior to reaching $r = r_{\text{int},c}$. The radial coordinate at which the equation of an antiatom's trajectory intersects that of the upper chamber boundary, $r_{\text{int},b}$, is found by evaluating Eq. (3) at $r = r_{\text{int},b}$ and equating the result to Eq. (9),

$$\frac{r_{\text{int},b} v_{0z}}{v_{0r}} - \frac{g r_{\text{int},b}^2}{2 v_{0r}^2} = a. \tag{14}$$

The two solutions for $r_{\text{int},b}$ are then

$$r_{\text{int},b,1,2} = \frac{v_{0r}\left(v_{0z} \pm \sqrt{v_{0z}^2 - 2ga}\right)}{g}. \tag{15}$$

If both $r_{\text{int},b,1,2} > r_{\text{int},c}$, the antiatom annihilates with the lower detector cone at $r = r_{\text{int},c}$, resulting in detection. The probability, P, of detection is given by

$$P = \frac{N_d}{N_{\bar{H}}}, \tag{16}$$

where N_d and $N_{\bar{H}}$ are the total number of recorded detections and simulated antiatoms, respectively.

A temperature of $T = 4$ K is assumed upon the basis that no antiproton plasma has ever been cooled to any significant degree below this value for the lowest such reported temperature is 3.5 K as experimentally achieved by the ATRAP collaboration.[7] The radius and half-height of the vacuum chamber are both defined to be $a = 0.6$ m in consideration of the spatial constraints for the experimental apparatus. Each simulation is performed with $N_{\bar{H}} = 10^8$ simulated antiatoms, unless otherwise noted.

PARAMETER OPTIMIZATION

A parameter optimization of the detector cones is conducted to determine the optimal experimental configuration. The domain of all possible values for the angle of each detector cone, θ_c, is defined as

$$\left\{\theta_c \middle| -\frac{\pi}{2} < \theta_c < \frac{\pi}{2},\ \theta_c = \frac{k\pi}{32},\ k \in \mathrm{Z}\right\}, \tag{17}$$

accounting for the physical limitations of the experimental apparatus. A single detector cone is initially considered and its angle varied over the domain. For each value of θ_c, the simulation is executed and the associated value of P recorded. The angle at which P obtains its maximum value is found and set to be the optimal value of θ_c. Within every sector subsequently formed by the optimized detector cone, a new detector cone is added and its respective angle likewise optimized for maximum P over the domain bounded by its sector. The optimization procedure is then iterated for each resulting sector formed by the optimized detector cones of the previous iteration until there exists a detector cone for every angle defined on the domain. Table 1 shows the values of θ_c and P for each optimized detector cone, indicated by the number of the iteration followed by a letter, in alphabetical order of greatest to least $\theta_{s,\max}$, denoting the sector in which the detector cone is optimized relative to the corresponding sectors of the other optimized detector cones of the same iteration.

At the conclusion of each iteration n, 10 simulations are performed including the optimized detector cones of all iterations up to n. The average value, $\langle P \rangle$, and standard deviation, σ_P, of the probability of detection are calculated and the results are shown in Table 2.

TABLE 1. Angle, θ_c, and associated probability of detection, P, for each optimized detector cone.

Cone	**1a**	**2a**	**2b**	**3a**	**3b**	**4a**	**4b**
θ_c	$\pi/32$	$\pi/16$	0	$3\pi/32$	$-\pi/32$	$5\pi/32$	$-\pi/16$
P	4.49×10^{-5}	8.77×10^{-5}	8.95×10^{-5}	1.73×10^{-4}	1.77×10^{-4}	2.57×10^{-4}	2.60×10^{-4}
Cone	**5a**	**5b**	**5c**	**6a**	**6b**	**7a**	**7b**
θ_c	$3\pi/16$	$\pi/8$	$-3\pi/32$	$7\pi/32$	$-\pi/8$	$\pi/4$	$-5\pi/32$
P	3.33×10^{-4}	3.37×10^{-4}	3.42×10^{-4}	4.55×10^{-4}	4.59×10^{-4}	5.25×10^{-4}	5.31×10^{-4}
Cone	**8a**	**8b**	**9a**	**9b**	**10a**	**10b**	**10c**
θ_c	$9\pi/32$	$-3\pi/16$	$5\pi/16$	$-\pi/4$	$11\pi/32$	$-7\pi/32$	$-9\pi/32$
P	5.87×10^{-4}	5.98×10^{-4}	6.35×10^{-4}	6.54×10^{-4}	6.75×10^{-4}	7.00×10^{-4}	6.95×10^{-4}
Cone	**11a**	**11b**	**12a**	**12b**	**13a**	**13b**	**13c**
θ_c	$3\pi/8$	$-5\pi/16$	$13\pi/32$	$-13\pi/32$	$15\pi/32$	$-11\pi/32$	$-15\pi/32$
P	7.44×10^{-4}	7.48×10^{-4}	7.61×10^{-4}	7.66×10^{-4}	7.69×10^{-4}	7.76×10^{-4}	7.69×10^{-4}
Cone	**14a**	**14b**	**14c**	**-**	**-**	**-**	**-**
θ_c	$7\pi/16$	$-3\pi/8$	$-7\pi/16$	-	-	-	-
P	7.83×10^{-4}	7.81×10^{-4}	7.80×10^{-4}	-	-	-	-

TABLE 2. Average value, $\langle P \rangle$, and standard deviation, σ_P, of the probability of detection for each iteration n.

n	1	2	3	4	5	6	7
$\langle P \rangle$	4.42×10^{-5}	1.31×10^{-4}	2.16×10^{-4}	2.99×10^{-4}	4.17×10^{-4}	4.92×10^{-4}	5.61×10^{-4}
σ_p	6.64×10^{-7}	1.03×10^{-6}	2.22×10^{-6}	1.48×10^{-6}	1.71×10^{-6}	1.95×10^{-6}	2.40×10^{-6}
n	**8**	**9**	**10**	**11**	**12**	**13**	**14**
$\langle P \rangle$	6.19×10^{-4}	6.66×10^{-4}	7.37×10^{-4}	7.58×10^{-4}	7.66×10^{-4}	7.77×10^{-4}	7.88×10^{-4}
σ_p	4.05×10^{-6}	3.11×10^{-6}	2.54×10^{-6}	3.10×10^{-6}	3.22×10^{-6}	2.96×10^{-6}	2.02×10^{-6}

Figure 3(a) shows the relationship between $\langle P \rangle$ and n, which increases linearly for $1 \le n \le 10$ and behaves asymptotically for $10 \le n < 14$. The optimal experimental configuration is defined to be $n = 10$, in consideration of the tradeoff between maximizing the signal and minimizing the experimental complexity. The trajectories and sites of annihilation of antiatoms that annihilate with the detector cones of the optimal experimental configuration for $N_{\bar{H}} = 100{,}000$ simulated antiatoms are shown in Fig. 3(b). It is observed that the trajectories tend to follow almost straight paths close to the lower detector cones of each sector and further that the greatest frequency of annihilations occurs near the r-axis.

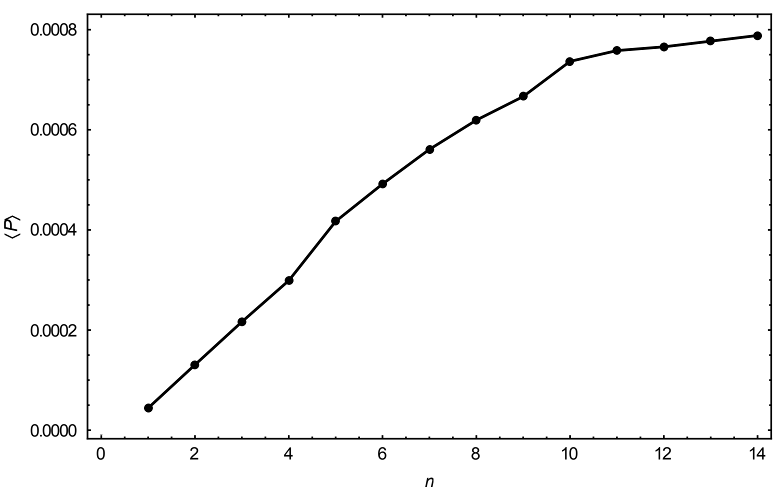

(a)

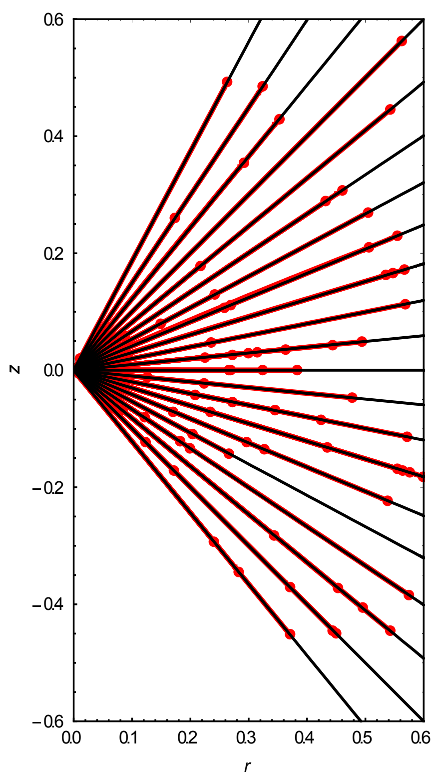

(b)

FIGURE 3. (a) Relationship between the average probability of detection, $\langle P \rangle$, and the number of the iteration, n. (b) Trajectories and sites of annihilation of antiatoms that annihilate with the detector cones of the optimal experimental configuration for $N_{\bar{H}} = 100{,}000$ simulated antiatoms.

DISCUSSION AND CONCLUSION

The residual gas pressure inside the vacuum chamber must be sufficiently low. If the mean free path of antihydrogen inside the chamber is too small, the resulting noise would mask the asymmetry of a signal that would otherwise indicate the direction of antihydrogen acceleration due to gravity. An estimate of a feasible lower limit for the residual gas pressure inside of the vacuum chamber is difficult, because the chamber would be maintained at a cryogenic temperature and because of many other factors that may be important. For collisions between antihydrogen and hydrogen atoms at collision energies of ~ 1 K in temperature units, the annihilation cross section and elastic scattering cross section are typically within an order of magnitude of each other.[8] For simplicity, the same will be assumed for collisions between antihydrogen and other possible residual gas particles, although information is lacking. A sufficiently long antihydrogen mean free path would then be associated with a long antihydrogen lifetime under conditions where antihydrogen is magnetically trapped. The ATRAP collaboration has claimed the achievement of a vacuum chamber pressure as low as 6×10^{-17} torr in a 1.2 K environment, which would allow antihydrogen storage times of over 1 year.[9] Such a vacuum chamber pressure may be considered a lower limit, with a density of residual gas particles small enough to have a negligible effect on antihydrogen during typical experimental timescales. Also, a recent analysis by the ALPHA collaboration indicates that a preliminary lower limit of the lifetime of trapped antihydrogen in the ALPHA-2 magnetic trap is 66 hours.[6]

A Monte Carlo simulation and parameter optimization have been presented of a concentric cone antihydrogen gravity experiment. It is found that for the given parameters, the optimal experimental configuration yields an average probability of detection of $\langle P \rangle = 7.37\times10^{-4}$, corresponding to the minimum production of approximately 1357 antiatoms necessary for the experiment to determine the direction of the gravitational acceleration of antihydrogen. The study therefore indicates that a substantial reduction in the required number of antiatoms may be possible relative to that of previously proposed aperture-based antihydrogen gravity experiments.

ACKNOWLEDGMENTS

This material is based upon work supported by the National Science Foundation under Grant No. PHY-1500427 and PHY-1803047 and by the Department of Energy under Grant No. DE-FG02-06ER54883.

REFERENCES

1. P. Scampoli and J. Storey, Mod. Phys. Lett. A 29, 1430017 (2014).
2. A. I. Zhmoginov, A. E. Charman, R. Shalloo, J. Fajans, and J. S. Wurtele, Classical and Quantum Gravity 30, 205014. (2013).
3. P. Perez, D. Banerjee, F. Biraben, D. Brook-Roberge, M. Charlton, P. Cladé, et al., Hyperfine Interactions 233, 21-27 (2015).
4. A.H. Treacher, R.M. Hedlof, C.A. Ordonez, Physics Procedia 66, 180-185 (2015).
5. J. R. Rocha, R. M. Hedlof, and C.A. Ordonez, AIP Advances 3, 102129 (2013).
6. A. Capra and ALPHA Collaboration, Hyperfine Interactions 240, 9 (2019).
7. G. Gabrielse, W. S. Kolthammer, R. McConnell, P. Richerme, R. Kalra, E. Novitski, D. Grzonka, W. Oelert, T. Sefzick, M. Zielinski, D. Fitzakerley, M. C. George, E. A. Hessels, C. H. Storry, M. Weel, A. Mullers, and J. Walz, Phys. Rev. Lett. 106, 073002 (2011).
8. P. Froelich, S. Jonsell, A. Saenz, B. Zygelman, and A. Dalgarno, Phys. Rev. Lett. 84, 4577 (2000).
9. D. W. Fitzakerley, M. C. George, E. A. Hessels, C. H. Storry, M. Weel, D. Grzonka, W. Oelert, G. Gabrielse, W. S. Kolthammer, R. Mcconnell, P. Richerme, J. Walz, Bulletin of the American Physical Society 58, Q1.00129 (2013). http://meetings.aps.org/link/BAPS.2013.DAMOP.Q1.129